# Immobilization of Magnetic Magnetite Nanoparticle Film on Polyamide Fabric

**H. Zhang, J. Y. Zheng**

*School of Textiles and Materials, Xi'an Polytechnic University, Xi'an Shaanxi 710048, China*

Received 22 November 2010; accepted 23 November 2011
DOI 10.1002/app.36536
Published online in Wiley Online Library (wileyonlinelibrary.com).

**ABSTRACT:** Polyamide (PA) fabric loaded with magnetite ($Fe_3O_4$) nanoparticle film was prepared by a simple chemical coprecipitation method. The surface morphology, chemical and phase constituents, crystalline structure, magnetic behavior, thermal stability, and mechanical properties of the $Fe_3O_4$-coated fabric were determined by means of scanning electron microscopy, energy-dispersive X-ray spectroscopy, X-ray diffraction, vibrating sample magnetometry, thermogravimetric analysis, differential scanning calorimetry, Fourier transform infrared spectroscopy, and tensile testing. The results show that a thin membrane of $Fe_3O_4$ nanoparticles was immobilized on the surface of THE PA fabric. The saturation magnetization of the $Fe_3O_4$-coated fabric was 27.5 emu/g. The onset decomposition temperature increased slightly, but the initial endothermic temperature decreased. The $Fe_3O_4$ nanoparticles were deposited on the fiber surface by mechanical anchoring action. © 2012 Wiley Periodicals, Inc. J Appl Polym Sci 000: 000–000, 2012

**Key words:** magnetic polymers; modification; nanotechnology; polyamides

## INTRODUCTION

Recently, iron oxide and ferrite on the ultrananoscale have attracted worldwide research attention because of their extraordinary features, including superparamagnetism, high field reversibility, high saturation field, extra anisotropy contributions, shifted loops after field cooling, and blocking temperature. On the basis of their unique properties, superparamagnetic nanoparticles offer many potential applications in a variety of fields, such as in high-density data storage, biomedicine, controlled drug delivery, electromagnetic shielding, magnetic refrigeration, multiply printing papers, catalysts, and ferrofluids.[1]

Magnetite ($Fe_3O_4$), as an important member of half-metallic materials, has a cubic inverse spinel structure, with oxygen forming face-centered cubic (fcc) closed packing and Fe cations occupying interstitial tetrahedral sites and octahedral sites.[2–4] Magnetite has been widely used in industrial and biomedical applications because of its excellent magnetic properties, high chemical stability, and exceptional biocompatibility.[5] Many approaches have been developed for the synthesis of magnetic $Fe_3O_4$ nanoparticles, including ball milling, the sol–gel method, thermal decomposition, sonochemical synthesis, chemical precipitation, hydrothermal synthesis, the microemulsion method, solventless thermal decomposition, high-temperature reflux, ultrasonic irradiation synthesis, and polymer template methods.[6] Although the coprecipitation method presents slow control of the particle shape, broad distributions of sizes, and aggregation of particles, the coprecipitation of ferrous and ferric salts by different inorganic bases from solution is the most convenient and simplest procedure. The synthesis of $Fe_3O_4$ through chemical precipitation includes: (1) coprecipitation of $Fe^{3+}$ and $Fe^{2+}$, (2) partial reduction of $Fe^{3+}$, and (3) partial oxidation of $Fe^{2+}$ followed by coprecipitation with ammonium hydroxide ($NH_3{\cdot}H_2O$) in water and in alcohol or with NaOH in water. Ferrous and ferric chlorides or sulfates are usually used as the iron source.[7,8] The aqueous coprecipitation of $Fe^{3+}:Fe^{2+} \leq 2:1$ (molar ratio) to prepare $Fe_3O_4$ nanoparticles is usually carried out in the presence of a base at pH 9–12 in an anaerobic or air environment.[9,10] $Fe_3O_4$ particle–chain microwires were synthesized under a magnetic field by a simple coprecipitation method. The increase in the magnetic field caused the lengthening of the wires.[11]

Unfortunately, $Fe_3O_4$ is highly susceptible to oxidation when it is exposed to the atmosphere. Furthermore, $Fe_3O_4$ nanoparticles aggregate seriously because of their large surface area-to-volume ratio and magnetic dipole–dipole attractions. Therefore, one of the main problems in producing stable magnetic fluids is the agglomeration during the synthesis and coating processes.[12] It has been

*Correspondence to:* H. Zhang (hzhangw532@xpu.edu.cn).

demonstrated that the formation of a passive coating of inert materials, such as organic polymers and inorganic materials, on the surfaces of $Fe_3O_4$ nanoparticles could help to prevent their aggregation in a dispersant and improve their chemical reactivity and stability.[13] Well-dispersed $Fe_3O_4$ nanoparticles have been achieved by the functionalization of magnetic particles through organic vapor condensation, polymer coating, surfactant adsorption, and direct silylation with silane coupling agents.[14–21] The coexisting surfactants remarkably influenced both the formation of crystalline nuclei and the dispersion stabilization of the formed precipitates.[22,23]

Magnetic fibers can be prepared either by lumen loading or by the *in situ* synthesis of ferrites. For the lumen loading process, commercially available magnetic $Fe_3O_4$ or $Fe_2O_3$ pigments were introduced into the lumens of cellulose fibers.[24–27] To improve the lumen loading degree, aluminum sulfate (alum) and polyethylenimine as retention aids were used throughout the experiment and were found to be beneficial in the preparation of this magnetic pulp.[28] Magnetic fibers can also be prepared via the *in situ* synthesis of ferrite in the presence of fibers. However, this method produced some nonmagnetic iron oxy–hydroxides, which would detrimentally affect the magnetic properties.[29–38] For instance, the filaments of a tire cord rayon were rendered magnetic by the *in situ* synthesis of ferrites.[39] The amount of the alkali, the pH value, and the reaction temperature influenced the magnetite formation.[40–43] Metal hydroxides precipitated within the polymer matrix without addition of a base or an oxidizer because the polymer imine groups provided a basic medium.[44]

In this work, we report the fabrication of magnetic $Fe_3O_4$ nanoparticle film on polyamide (PA) fabric. Magnetic $Fe_3O_4$ nanoparticles were prepared by the coprecipitation of $Fe^{2+}$ and $Fe^{3+}$ with ammonium hydroxide as a precipitating agent; meanwhile, the nanoparticles were deposited on the surface of PA fiber. The surface morphology, chemical and phase constituents, crystalline structure, magnetic behavior, and thermal stability of $Fe_3O_4$-coated fabric were characterized by scanning electron microscopy (SEM), energy-dispersive X-ray spectroscopy (EDX), X-ray diffraction (XRD), vibrating sample magnetometry (VSM), thermogravimetric analysis (TGA), differential scanning calorimetry (DSC), and Fourier transform infrared (FTIR) spectroscopy. The effects of the $Fe_3O_4$ nanoparticle coating on the bonding strength and tensile properties of the PA fabric were also investigated. As shown by the results, this preparation could be a low-cost way for producing magnetic fabrics deposited with $Fe_3O_4$ nanoparticles, which would provide a great opportunity for the application of magnetite powders in clothing.

## EXPERIMENTAL

### Materials

Undyed plain woven PA fabric was used for loading with the $Fe_3O_4$ nanoparticles; it was obtained from Guangdong Xinhui Meida Nylon Co., Ltd., Jianmen city, Guangdong province, China. The linear densities of the ends and picks were identical (9.4 tex). The numbers of the ends and picks were 390 and 300 per 10 cm, respectively. The chemicals used, including ferric trichloride hexahydrate ($FeCl_3{\cdot}6H_2O$), ferrous chloride tetrahydrate ($FeCl_2{\cdot}4H_2O$), $NH_3{\cdot}H_2O$, 36% hydrochloric acid (HCl), and deionized water, were all analytical-reagent grade.

### Preparation of the ferroferric oxide films on the PA fabric

The PA fabric sample (1.5 g) was etched in a 200 mL/L hydrochloric acid solution at room temperature for 15 min and then rinsed in deionized water completely. The coprecipitation technique was employed to prepare $Fe_3O_4$ nanoparticles, which was immobilized on the surface of the PA fiber. $FeCl_2{\cdot}4H_2O$ (1.24 g) and $FeCl_3{\cdot}6H_2O$ (0.9 g) were first dissolved in 750 mL of deionized water at a temperature of 30°C. The molar ratio of $FeCl_3$ to $FeCl_2$ was 2: 1. The concentration of $Fe^{2+}$ and $Fe^{3+}$ was 0.05 mol/L. Subsequently, the pretreated fabric sample was immersed in the aforementioned solution. Finally, 28 mass % aqueous ammonia was added dropwise, and after that, the mixture was vigorously stirred at 500 rpm. The pH was adjusted to 9. When the color of the suspension gradually turned from salmon pink to brown and suddenly to black, the process of dropping was sustained to maintain a pH of 9. Stirring was continued to complete the reaction. After 2 h of stirring at 30°C, the fabric sample was dried at 60°C for 5 min in a vacuum oven and then washed 20 times with deionized water at 80°C. The sample was dipped in the acetone and ethanol solutions twice for 10 min, respectively, then washed with deionized water three times for 10 min, and dried at 40°C. The black precipitates were separated by centrifugation and then washed with deionized water until the pH was neutral. The collected powders were dried in a vacuum atmosphere at 60°C for 24 h.

### Characterization methods

#### SEM and EDX

The surface morphologies of the samples were observed with a JEOL JSM-6700 field emission scanning electron microscope, JEOL Ltd, Tokyo, Japan, equipped with an Oxford INCA Energy 400 energy-dispersive X-ray spectrometer, Oxford instruments,

Oxford, UK. The sample was mounted on SEM stubs and sputter-coated with platinum before examination. The SEM images of the fabric surface and the powders were measured randomly. The particle size was analyzed with the attached software. The EDX survey spectrum of the $Fe_3O_4$-coated sample was performed with the energy-dispersive spectrometer.

### XRD testing

XRD patterns were obtained with Cu $K\alpha_1$ radiation ($\lambda = 1.540562$ Å) and with a 7000S diffractometer, Rigaku Corporation, Tokyo, Japan, at 40 kV and 40 mA with the angle of $2\theta$ from 20 to 80° at a scanning speed of 10 deg/min. The mean crystallite size of the $Fe_3O_4$ particles formed on the surface of the PA fabric was determined by the Scherrer equation:

$$D = K\lambda/\beta \cos \theta$$

where $D$ is the diameter of the particles, $\lambda$ is the X-ray wavelength, $\beta$ is the full width at half-maximum of the diffraction line, $\theta$ is the diffraction angle, and $K$ is a constant (0.89).

### VSM testing

The static magnetic properties of the $Fe_3O_4$ particles and the $Fe_3O_4$-coated fabric were measured with a vibrating sample magnetometer (Quantum design. Inc., San Diego, USA) at ambient temperature.

### TGA and DSC testing

TGA was carried out on a TGA/SDTA851e TGA/differential thermal analysis instrument, Mettler-Toledo Group, Schweiz, Switzerland, according to GB/T 13464–2008. The percentage weight change versus temperature was evaluated at a heating rate of 10°/min with a nitrogen flush rate of 10 mL/min over the range 40–550°C. DSC analyses were performed in a Sapphire apparatus, Perkin Elmer, Inc., Massachusetts, USA, at a rate of 10°/min in flowing nitrogen gas at 10 mL/min from 40 to 550°C.

### FTIR spectrometry

The FTIR spectra of PA fabric samples before and after treatments were recorded with KBr pellets in the range 400–4000 $cm^{-1}$ and with a Bruker TENSOR 27 spectrometer, Bruker Optics Inc., Ettlingen, Germany.

### Fabric tensile testing

The tensile properties of the fabric samples were measured on a YG(B)026D-500 electromechanical test instrument, Wenzhou Darong Textile Instrument Co., Ltd., Wenzhou City, Jiangsu Province, China, according to GB/T3923.1-1997. The initial gauge length was 200 mm, and the width was 50 mm. The testing rate was 100 mm/min, and the pretension was 2 N.

### Attachment strength measurement

The attachment strength measurement was conducted according to GB/T8629-2001. The $Fe_3O_4$-coated fabric was washed in water with 1993 AATCC standard detergent without optical brightener at 40°C for 15 min, then rinsed with tap water for 3 min, and subsequently dried at 60°C in an oven. The procedure was repeated for 30 cycles, and then, the sample was weighed with a precision electronic balance with an accuracy of 0.01 mg (Sartorius Weighing Technology GmbH, Goettingen, Germany). The average percentage weight loss of the $Fe_3O_4$ film with respect to its initial weight was calculated. The change in the surface properties of the washed fabric was determined with the same scanning electron microscope.

## RESULTS AND DISCUSSION

### SEM analysis

The scanning electron micrographs of the PA fibers before and after treatment and the powder are shown in Figure 1. It can be seen that the surface of the original PA fiber was very clean but rough [see Fig. 1(a)]. Cracks and cavities were observed on the fiber surface because of the action of HCl [Fig. 1(b)]. When the PA fabric was treated by the chemical coprecipitation process, the surface of the as-obtained fiber was covered with a thin film composition. A few particles were attached to the fiber surface [Fig. 1(c)]. As shown in the high-resolution SEM image of the PA fiber, the particles deposited on the PA fiber surface were composed of nanoparticles with an average size of 25 nm [Fig. 1(d)]. The powders precipitated from the solution consisted of agglomerated nanoparticles with a spherical-like shape [Fig. 1(e)].

### EDX analysis

The nanoparticle-coated PA fabric was analyzed for its chemical compositions with an EDX spectrometer of an emissive-type electron microscope. The EDX survey spectrum of the particle coated fabric is illustrated in Figure 2. The EDX showed that the element was composed of O, Fe, and Pt. The mass percentages of O, Fe, and Pt were 19.55, 10.99, and 69.46, respectively. The corresponding atomic percentages were 68.85% O, 11.09% Fe, and 20.06% Pt.

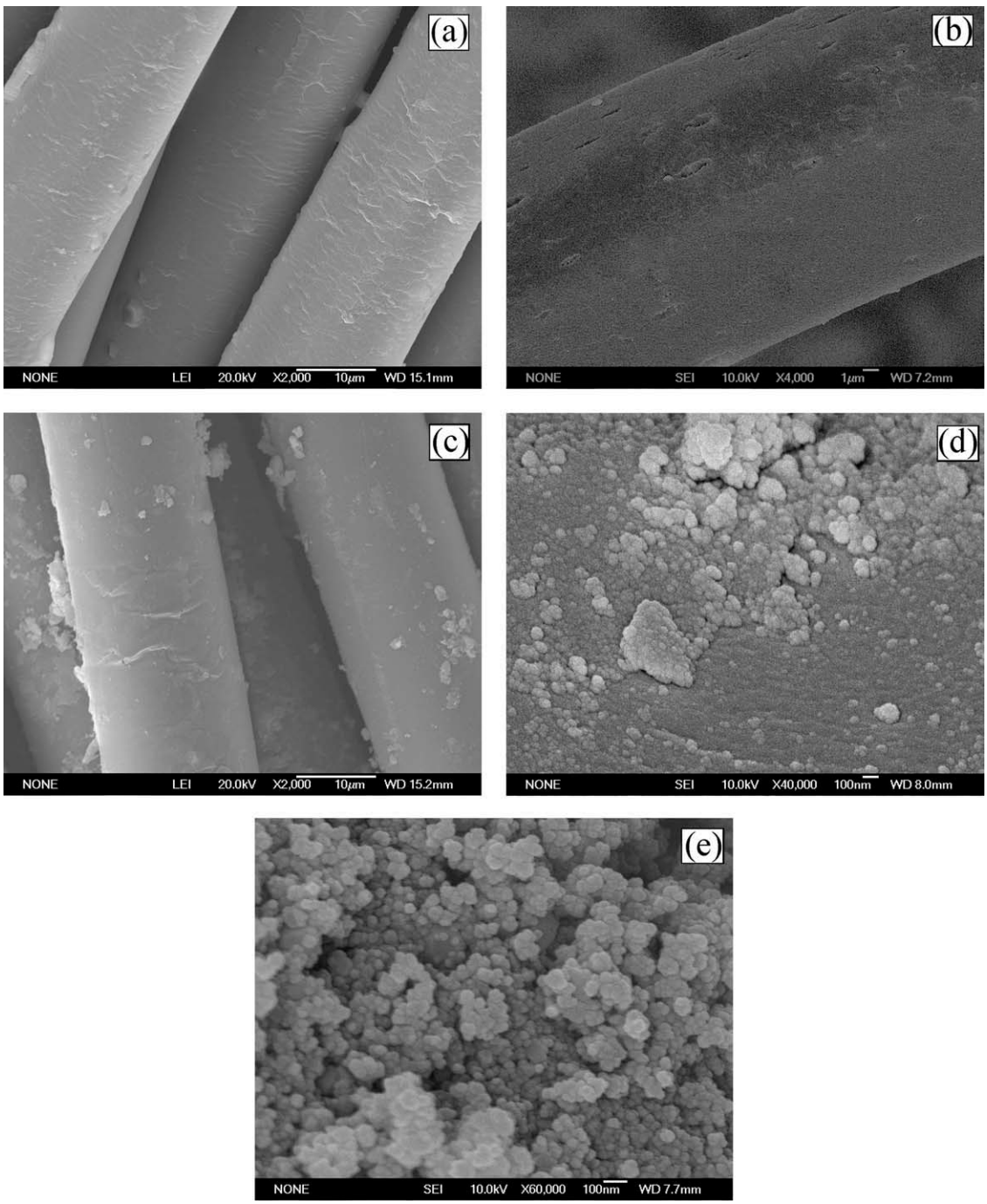


**Figure 1** SEM images of the (a) original PA fiber, (b) etched PA fiber, (c,d) $Fe_3O_4$-immobilized PA fibers at different magnifications, and (e) $Fe_3O_4$ powder.

### XRD analysis

The XRD patterns of the PA fabric before and after treatments and the powder are represented in Figure 3. It was clear that the intense diffraction peak at $2\theta = 22^\circ$ was due to the typical PA fiber phase. The diffraction peaks of the powder were well consistent with the data list in JCPDS Card no.19-0629; this indicated that it was the magnetic ferriferous oxide. As compared with the original PA fabric, the $Fe_3O_4$ phase was detected in the XRD pattern of the coated fabric; this confirmed that $Fe_3O_4$ nanoparticles were successfully immobilized on the fiber surface. A series of characteristic peaks were observed in the XRD pattern at $2\theta$ values of 28, 36, 43, 54, 57, 63, and 74°. These were related to the {220}, {311}, {400}, {422}, {511}, {440} and {533} planes, respectively, of the $Fe_3O_4$ cubic inverse spinel structure. From the width of the peak at $2\theta = 36^\circ$ (dominant crystal plane {311}), the crystallite size of the $Fe_3O_4$ particles

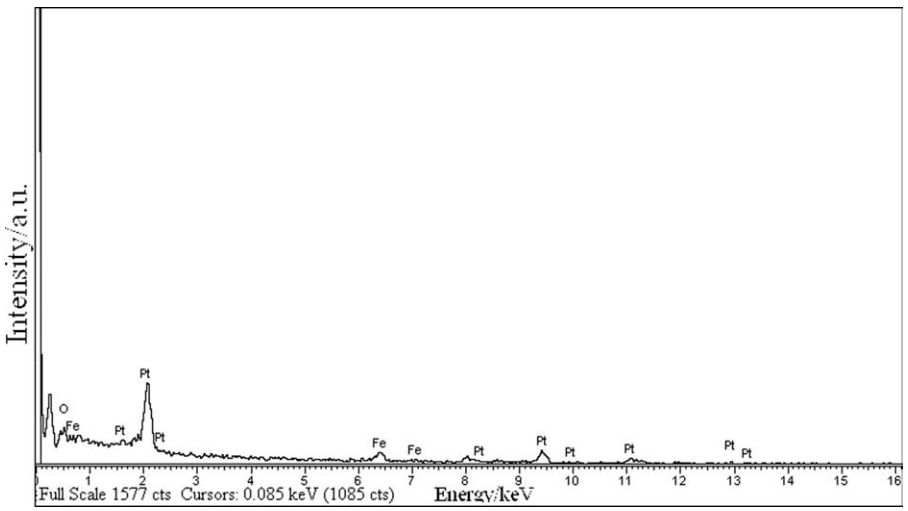


**Figure 2** EDX survey spectrum of the PA fabric immobilized with $Fe_3O_4$ nanoparticles.

was calculated to be 21.4 nm with Scherrer's equation. This was in good agreement with the particle size analysis by SEM.

### VSM analysis

The hysteresis loops of the $Fe_3O_4$ powder and the $Fe_3O_4$-coated fabric are displayed in Figure 4. It was obvious that the saturation magnetization of the $Fe_3O_4$ powder was 63 emu/g at room temperature. For the $Fe_3O_4$-coated fabric, the saturation magnetization was 27.5 emu/g. The remnant magnetizations for both samples were zero. The magnetic loop suggested that the synthesized $Fe_3O_4$ nanoparticles were possessed of superparamagnetism behavior. The particles showed high saturation magnetizations in the presence of a magnetic field. As soon as the magnetic field was switched off, the magnetization disappeared immediately.

### TGA

The TGA curves of the PA fabric before and after treatments are exhibited in Figure 5. It was evident that similar weight loss curves could be observed for both samples. When PA fabric was deposited with a layer of $Fe_3O_4$ nanoparticle film, the onset decomposition temperature increased from 386.6 to 392.1°C, and the endset decomposition temperature increased from 429.2 to 442.0°C. The corresponding weight loss decreased from 93.9 to 79.2% between 291.1 and 543.8°C. So the amount of $Fe_3O_4$ nanoparticles deposited on the PA fabric was estimated to be about 15% (w/w), regardless of the reaction among $Fe_3O_4$, PA fiber, and nitrogen gas.

### DSC analysis

The DSC curves of the PA fabric before and after treatments are presented in Figure 6. It was clear that

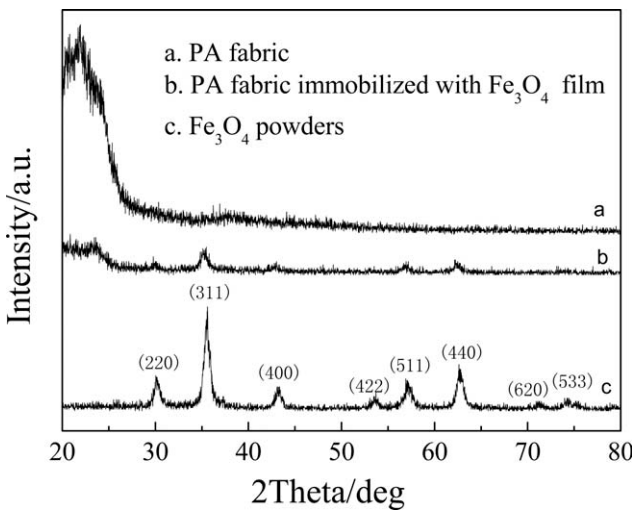


**Figure 3** XRD patterns of the PA fabric: (a) the original fabric, (b) the $Fe_3O_4$-coated fabric, and (c) the powder.

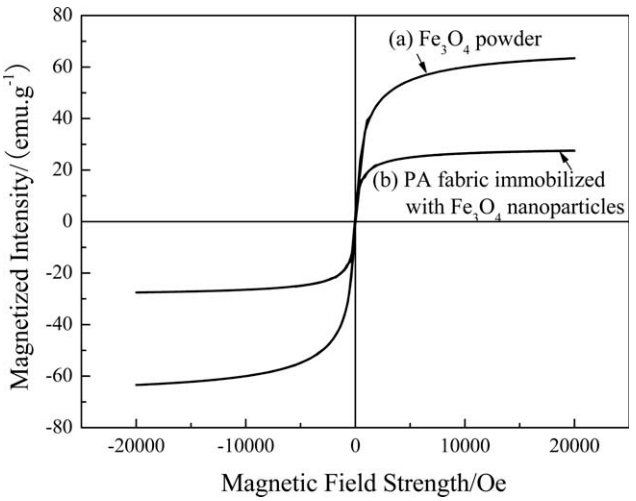


**Figure 4** Field-dependent magnetization at room temperature for the (a) $Fe_3O_4$ powder and (b) $Fe_3O_4$-coated fabric.

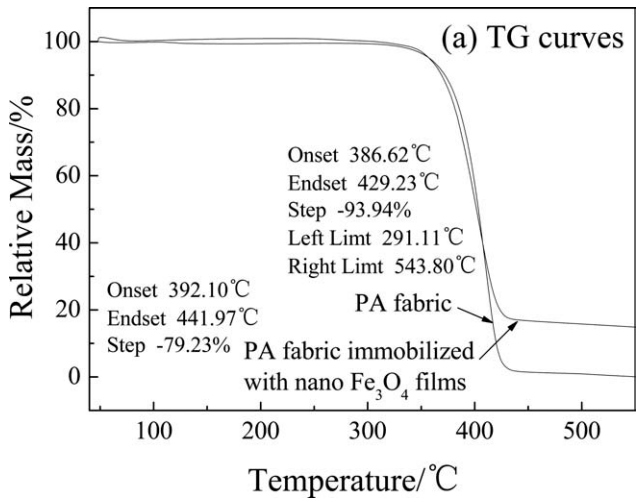


**Figure 5** TGA curves of the PA fabric before and after treatment. TG: thermal gravimetric.

the heat flow curve of the original fabric was quite different from that of the $Fe_3O_4$-coated sample. The endothermic peak at 226.2°C was reduced to 215.3°C when the PA fabric was covered with a film of $Fe_3O_4$ nanoparticles. The exothermic peak at 456.5°C was separated into two peaks at 453.0 and 458.8°C; this indicated the decomposition of the PA fiber. For the $Fe_3O_4$-coated fabric, endothermic peaks at 215.3, 322.7, 349.8, and 381.6°C were observed. Meanwhile, exothermic peaks at 355.2, 390.2, 430.7, and 482.6°C were also observed. Therefore, the thermal stability of the PA fiber was distinctly changed when the PA fabric was immobilized with $Fe_3O_4$ nanoparticles.

## FTIR analysis

The FTIR spectra of the PA fabric before and after treatments are shown in Figure 7. It was quite remarkable that the IR spectrum of the $Fe_3O_4$-coated fabric was totally dominated by the spectrum of the original one. The N—H band of the original fabric at 3318 $cm^{-1}$ was slightly intensified; this was attributed to the surface-absorbed water induced by $Fe_3O_4$ nanoparticles. The absorption bands at 3086, 2931, and 2860 $cm^{-1}$ were attributed to the stretching vibrations of the —$CH_2$ group. The peak at 1644 $cm^{-1}$ (C=O stretching) was attributed to the amide I band, and the amide II band at 1538 $cm^{-1}$ (N—H deformation) was also observed. The peak at 1462 $cm^{-1}$ was assigned to the bending vibrations of the C—H group. The absorption bands at 1370 and 1169 $cm^{-1}$ were assigned to the asymmetrical and symmetric stretching vibrations of the C—N group, respectively. The peaks at 1260 and 1199 $cm^{-1}$ were attributed to the amide III band (N—H deformation and C—N stretching). The peaks at 1119, 974, and 927 $cm^{-1}$ were assigned to the stretching vibrations of the C—C group. The absorption band at 730 $cm^{-1}$ was attributed to the rocking vibrations of the —$CH_2$ group. The peaks at 691 and 578 $cm^{-1}$ were attributed to the out-of-plane bending vibrations of the N—H group.[45,46] However, the characteristic stretching

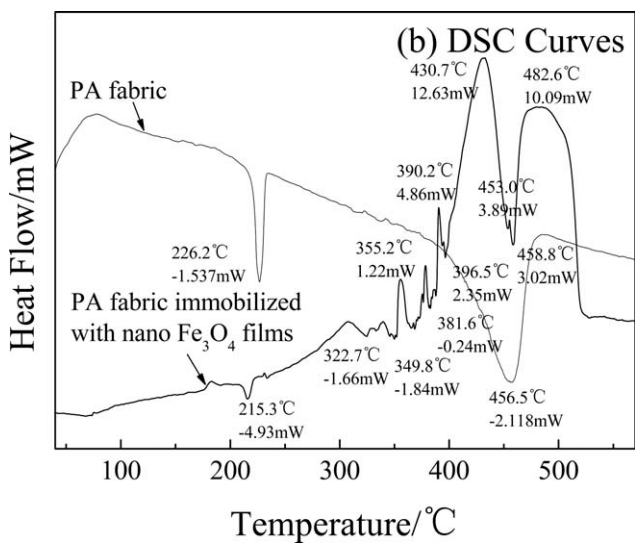


**Figure 6** DSC curves of the PA fabric before and after treatment.

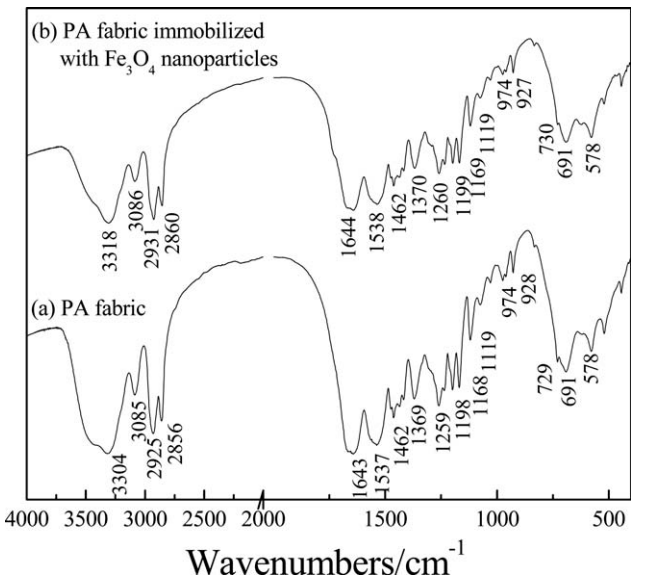


**Figure 7** FTIR curves of the PA fabric: (a) the original fabric and (b) the $Fe_3O_4$-coated fabric.

**TABLE I**
**Results of the Fabric Density and Tensile Property Testing of the PA Fabric before and after Treatment**

| | Density/ thread·(10 $cm^{-1}$) | | Breaking load (N) | | Tensile strain (%) | |
|---|---|---|---|---|---|---|
| PA fabric | Warp | Weft | Warp | Weft | Warp | Weft |
| Untreated | 390.0 | 300.0 | 781.0 | 479.0 | 42.9 | 44.6 |
| $Fe_3O_4$-coated | 446.0 | 350.0 | 777.0 | 401.0 | 34.5 | 27.5 |

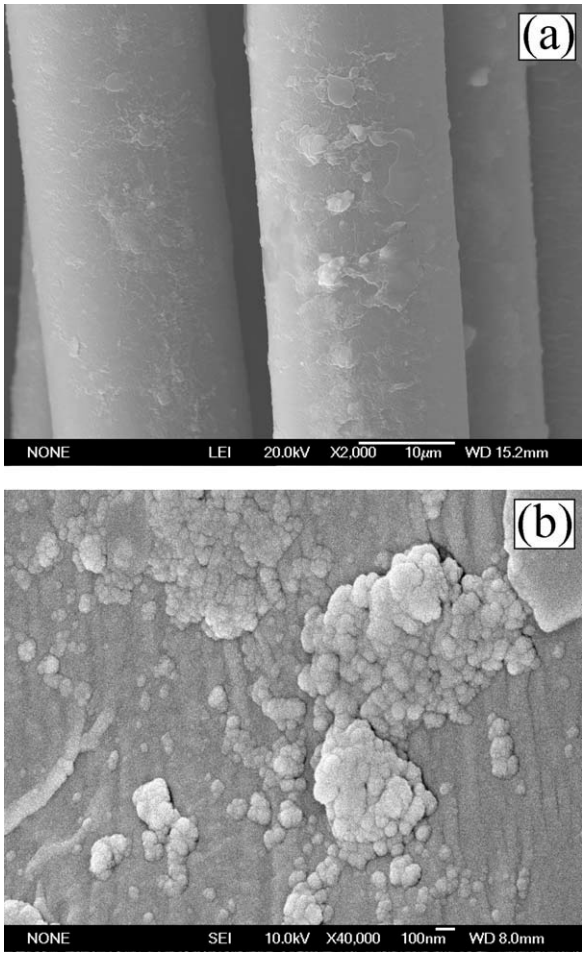


**Figure 8** SEM images of the $Fe_3O_4$-coated PA fiber after it was washed for 30 cycles: (a) 2000 and (b) 40,000×.

vibrations of the Fe–O band around 574 $cm^{-1}$ were negligible. This might have been due to the fact that the $Fe_3O_4$ nanoparticles grown on the PA fiber were present in a scarce amount, which was beyond the IR detection limitation. This indicated that the chemical structure of the PA fiber was not substantially changed. Although the $Fe_3O_4$-coated fabric was washed with organic solvents, the $Fe_3O_4$ nanoparticles were closely adhered onto the fiber surface.

### Tensile properties analyses

The tensile properties of the PA fabric before and after treatments are shown in Table I in accordance with GB/T3923.1-1997. The changes in the fabric densities are also given. The densities of the fabric in the warp and weft directions increased because the fabric was treated in an alkaline solution for a long time. The shrinkages of the PA fabric coated with the $Fe_3O_4$ nanoparticles film were about 12.6% in the warp direction and 14.3% in the weft direction, respectively. The breaking loads in the warp and weft directions decreased slightly. The tensile strains in both directions decreased to some extent.

### Attachment strength analysis

Less than a 0.05% weight loss was obtained for the $Fe_3O_4$-coated fabric after it was washed for 30 cycles. This suggested that the binding strength between the $Fe_3O_4$ nanoparticles and the PA fiber was enough to withstand the washing treatment. The SEM images of the washed sample are shown in Figure 8. It can be seen that the surface of the washed fiber became relatively clean compared with the unwashed one [Fig. 8(a)]. The $Fe_3O_4$ nanoparticles were closely adhered to the fiber surface, as shown in the high-resolution SEM image [Fig. 8(b)]. Combining this information with the analysis of FTIR, we inferred that the $Fe_3O_4$ nanoparticles were probably adhered by means of a mechanical anchoring action. The cracks and cavities played an important role in anchoring the $Fe_3O_4$ nanoparticles to the fiber surface. The $Fe_3O_4$ nanoparticle film propagation was initiated from these cracks and cavities, which was a fundamental prerequisite for the deposition of the $Fe_3O_4$ nanoparticles. So a sheath was formed on the fiber surface.

## CONCLUSIONS

To explore value-added textile products, a simple one-step preparation method for the fabrication of a magnetically responsive fabric was performed via the chemical coprecipitation process. Nanosized $Fe_3O_4$ particles were successfully precipitated in the presence of PA fabric and deposited on the fiber's surface by coprecipitation of ferric and ferrous iron at a molar ratio of 2: 1 under an air atmosphere. Synthesis tests demonstrated that it was feasible to prepare magnetic PA fabric by the coprecipitation method. SEM studies showed that the $Fe_3O_4$ nanoparticles looked spherical in shape. EDX and XRD studies demonstrated that the powder was magnetic ferriferous oxide less than 25 nm in average size. The particles were superparamagnetic, as determined by VSM. TGA and DSC studies indicated that the thermal stability of the PA fiber changed when the PA fabric was deposited with $Fe_3O_4$ nanoparticles. FTIR studies revealed that the chemical structure of the PA fiber was not changed. The mechanical properties of the $Fe_3O_4$-coated fabric decreased but not too much compared with the original one.

### References

1. Abareshi, M.; Goharshadi, E. K.; Zebarjad, S. M.; Fadafan, H. K.; Youssefi, A. J Magn Magn Mater 2010, 322, 3895.
2. Yanase, A.; Siratori, K. J Phys Soc Jpn 1984, 53, 312.
3. Zhang, Z.; Satpathy, S. Phys Rev B 1991, 44, 13319.
4. Dedkov, Y. S.; Rudiger, U.; Guntherodt, G. Phys Rev B 2002, 65, 64417.
5. Wu, J. H.; Ko, S. P.; Liu, H. L.; Kim, S.; Ju, J. S.; Kim, Y. K. Mater Lett 2007, 61, 3124.

6. Zhao, D. L.; Wang, X. X.; Zeng, X. W.; Xia, Q. S.; Tang, J. T. J Alloys Cmpd 2009, 477, 739.
7. Lee, S. J.; Jeong, J. R.; Shin, S. C.; Kim, J. C.; Kim, J. D. J Magn Magn Mater 2004, 282, 147.
8. Hong, R. Y.; Li, J. H.; Wang, J.; Li, H. Z. China Particuology 2007, 5, 186.
9. Wei, X. C.; Viadero, R. C., Jr. Colloids Surf A 2007, 294, 280.
10. Maity, D.; Agrawal, D. C. J Magn Magn Mater 2007, 308, 46.
11. Li, F. S.; Wang, Y.; Wang, T. J Solid State Chem 2007, 180, 1272.
12. Kim, D. K.; Zhang, Y.; Voit, W.; Rao, K. V.; Muhammed, M. J Magn Magn Mater 2001, 225, 30.
13. Chen, L. Y.; Xu, Z. X.; Dai, H.; Zhang, S. T. J Alloys Cmpd 2010, 497, 221.
14. Wooding, A.; Kilner, M.; Lambrick, D. B. IEEE Trans Magn 1988, 24, 1650.
15. Liu, Z. L.; Wang, H. B.; Lu, Q. H.; Du, G. H.; Peng, L.; Du, Y. Q.; Zhang, S. M.; Yao, K. L. J Magn Magn Mater 2004, 283, 258.
16. Hong, R. Y.; Zhang, S. Z.; Han, Y. P.; Li, H. Z.; Ding, J.; Zheng, Y. Powder Technol 2006, 170, 1.
17. Vidal-Vidal, J.; Rivas, J.; Lopez-Quintela, M. A. Colloids Surf A 2006, 288, 44.
18. Tao, K.; Dou, H. J.; Sun, K. Colloids Surf A 2006, 290, 70.
19. Tao, K.; Dou, H. J.; Sun, K. Colloids Surf A 2008, 320, 115.
20. Zhao, D. L.; Teng, P.; Xu, Y.; Xia, Q. S.; Tang, J. T. J Alloys Cmpd 2010, 502, 392.
21. Mahdavian, A. R.; Mirrahimi, M. A. Chem Eng J 2010, 159, 264.
22. Mizutani, N.; Iwasaki, T.; Watano, S.; Yanagida, T.; Kawai, T. Curr Appl Phys 2010, 10, 801.
23. Utech, S.; Scherer, C.; Krohne, K.; Carrella, L.; Rentschler, E.; Gasi, T.; Ksenofontov, V.; Felser, C.; Maskos, M. J Magn Magn Mater 2010, 322, 3519.
24. Marchessault, R. H.; Rioux, P.; Raymond, L. Polymer 1992, 33, 4024.
25. Rioux, P.; Ricard, S.; Marchessault, R. H. J Pulp Paper Sci 1992, 18, 39.
26. Zakaria, S.; Ong, B. H.; Ahmad, S. H.; Abdullah, M.; Yamauchi, T. Mater Chem Phys 2005, 89, 216.
27. Chia, C. H.; Zakaria, S.; Nguyen, K. L.; Abdullah, M. Ind Crops Prod 2008, 28, 333.
28. Zakaria, R. H.; Ricard, S.; Rioux, P. Carbohydr Res 1992, 224, 133.
30. Raymond, L.; Revol, J. F.; Ryan, D. H.; Marchessault, R. H. Chem Mater 1994, 6, 249.
31. Carrazana-García, J. A.; Lopez-Quintela, M. A.; Rivas-Rey, J. Colloids Surf A 1997, 121, 61.
32. Kim, D. K.; Zhang, Y.; Voit, W.; Rao, K. V.; Muhammed, M. J Magn Magn Mater 2001, 225, 30.
33. Pardoe, H.; Chua-Anusorn, W.; St. Pierre, T. G.; Dobson, J. J Magn Magn Mater 2001, 225, 41.
34. Chatterjee, J.; Haik, Y.; Chen, C. J. J Magn Magn Mater 2003, 257, 113.
35. Wang, J.; Zhang, K.; Peng, Z. M.; Chen, Q. W. J Crystal Growth 2004, 266, 500.
36. Giri, J.; Thakurta, G. T.; Bellare, J.; Nigam, A. K.; Bahadur, D. J Magn Magn Mater 2005, 293, 62.
37. Chia, C. H.; Zakaria, S.; Ahamd, S.; Abdullah, M.; Jani, S. M. Am J Appl Sci 2006, 3, 1750.
38. Munawar, R. F.; Zakaria, S.; Radiman, S.; Hua, C. C.; Abdullah, M.; Yamauchi, T. Sains Malaysiana 2010, 39, 593.
39. Raymond, L.; Revol, J. F.; Marchessault, R. H.; Ryan, D. H. Polymer 1995, 36, 5035.
40. Katsuhisa, F.; Masaaki, M. Jpn TAPPI J 2003, 57, 556.
41. Katsuhisa, F. Jpn TAPPI J 2003, 57, 416.
42. Tang, A. M.; Zhang, H. W.; Chen, G.; Liu, Y. Y. Trans China Pulp Pap 2006, 21, 66.
43. Small, A. C.; Johnston, J. H. J Colloid Interface Sci 2009, 331, 122.
44. Castro, C.; Ramos, J.; Millan, A.; Calbet, J. G.; Palacio, F. Chem Mater 2000, 12, 3681.
45. Pan, C. H.; Chien, J. Y. Acta Phys Sinica 1962, 18, 159.
46. Zhu, W. L. Plastics 2009, 38, 114.